

Li, B - BEHAVIOR IN LUNAR BASALTS DURING SHOCK & THERMAL METAMORPHISM:

IMPLICATIONS FOR H₂O IN MARTIAN MAGMAS Johny Chaklader¹ (jchaklad@unm.edu), C.K. Shearer¹ (cshearer@unm.edu), and F. Hörz². ¹Institute of Meteoritics, Department of Earth & Planetary Sciences, University of New Mexico, Albuquerque, NM 87131-1126. ²NASA Johnson Space Center, Houston, Texas 77058.

Introduction: The water-content of Martian magmas is a topic of debate among researchers. Some Martian basalts are characterized with melt inclusions of biotite, apatite and amphibole; phases typically associated with hydration reactions on Earth [1-3]. However, the H-content of melt inclusions from these basalts is low, and bulk-rock H₂O-contents range from a meager 0.013 to 0.035 wt. % in Shergotty [4]. Nonetheless, researchers note that low present-day water contents do not preclude a once hydrous past [5]. Since light lithophile elements (LLE), such as Li and B, partition into aqueous fluids at T > 350 °C, workers proposed that Li-B depletions in pyroxene rims of Nakhilite and Shergottite basalts reflect the loss of several weight percent water from Martian magmas during crystallization [6]. Since similar depletions were observed in pyroxene rims from completely dry lunar basalts, it is likely that alternative mechanisms also contribute to the distribution of elements such as Li and B [7]. Given that many Martian basalts have experienced considerable shock pressures (15-45 GPa), it is possible that shock and subsequent thermal metamorphism may have influenced the volatile element records of these basalts [8]. In order to better understand the distribution of Li and B, we are studying the effects of crystal chemistry, shock pressure, and thermal metamorphism in pyroxenes from lunar basalts. Below, we discuss results from experimentally shocked and thermally metamorphosed Apollo 11, 10017 (A-11) and Apollo 17, 75035 (A-17) basalts.

Methods: A-11 and A-17 high-Ti basalts were experimentally shocked at the Johnson Space Center as described by [9]. An unshocked sample of A-11 basalt was heated under vacuum (~10⁻⁴ atm) following the approach of [10,11]. Pyroxenes were imaged with a JEOL JSM-5800 LV SEM and analyzed with a JEOL JXA-8200 EMP using a 0.5 μm beam diameter, 20 kv accelerating voltage and 20 nA current. Pyroxenes were analyzed for ⁷Li, ⁹Be, ¹¹B, ⁸⁸Sr, ¹⁴⁰Ce, ¹⁴⁶Nd, and ¹⁷⁴Yb using a Cameca ims 4f. Thin sections were soaked in 1 % mannitol solution, rinsed in ultrapure (18 MΩ) water and rastered to reduce effects of B contamination. Analyses were made by bombarding samples with a 15 nA current of primary O⁻ ions under a 10 kv potential focused to a 10-15 μm spot diameter. Sputtered secondary ions were energy filtered with a sample offset voltage of 75 V and an energy window of ±25 V. The effect of ²⁷Al³⁺ on ⁹Be was investigated by analyzing ⁹Be at a higher mass resolution.

Sample Description: Unshocked A-11 sample is a high-Ti, low-K, medium grained, subophitic basalt with abundant clinopyroxene, calcic plagioclase, ilmenite, minor interstitial glass and pyroxferroite. Unshocked A-17 sample is a high-Ti, medium-grained, subophitic basalt consisting of clinopyroxene, calcic plagioclase, ilmenite, cristobalite, pyroxferroite, native iron, troilite, and some mesostasis. Both basalts crystallized at $fO_2 \approx IW - 1$ under extremely dry conditions [12]. A-11 and A-17 basalts were shocked at the JSC at pressures ranging 34.8 to 78.5 GPa and 9.3 to 99.9 GPa, respectively [9]. A sample of A-11 basalt was heated for 7 days at 1000° C [10,11].

Results & Discussion: Results show that mechanisms of coupled substitution utilized by major and minor elements are important to the distribution of LLE in pyroxenes. All pyroxenes express well-defined compositional zoning with augitic cores and pigeonite rims in pyroxene quadrilateral components (Figures 1, 2). A-17 pyroxenes exhibit a more extensive enrichment in Fe-content than A-11 pyroxenes. Shock does not affect zoning in En, Fs, and Wo-components. Figure 3 shows that pyroxene cores are enriched in Ti and Al relative to rims. A-17 analyses plot tightly along the line of ½ slope, irrespective of shock pressure or distance along transect, showing a clear preference for coupled substitution mechanism: $[(Ti^{4+})^{VI} + 2(Al^{3+})^{IV}] \leftrightarrow [(R^{2+})^{VI} + 2Si^{IV}]$ [13]. This mechanism is also dominant for A-11 pyroxenes. Furthermore, results suggest that Ti-Al partitioning is more important at higher Ca-contents (Figure 4). Ca is a large M2-site cation (>0.10 nm S-P ionic radius) that likely stretches neighboring M1 and tetrahedral sites, thus facilitating substitution of the Ti-Al couple. Figures 5 and 6 illustrate plots of Li vs. Li/Ce and B vs. B/Ce, respectively. Ce is a light REE and behaves incompatibly, increasing in concentration toward rims. Pyroxene rims are depleted in Li and B, expressing lower Li/Ce and B/Ce values than cores. Late-stage Li-partitioning into pyroxenes may be affected by decreases in Ca-content (Figure 7). Ca influences the behavior of Al, which in turn can substitute as an octahedrally coordinated cation that couples with Li for respective M1 and M2-site occupancy. For example, Figure 8 shows that pyroxenes with higher Li-contents have greater abundances of octahedrally coordinated Al. These observations are not consistent with the experimental results of [14], which support limited Ca and Al affects on Li and B partitioning. Alternatively,

results of this work also document the coupled substitution of Li (M2) and Cr³⁺ (M1) during pyroxene crystallization. In these pyroxenes, loss of Cr occurs with increasing degrees of crystallization. With decreasing Cr-content, Li-partitioning was less significant during rim formation than during earlier periods of Cr-availability. It is noteworthy that Cr was not included in the starting compositions of [14]. Higher shock pressures can significantly redistribute B in pyroxenes but have no notable effects on Li. It is likely that shock and subsequent thermal metamorphism facilitate Li-B mobility among melt inclusions, pyroxene grains and zones of surrounding mesostasis. Measurements indicate that mesostasis contains up to 50 times more Li and B than pyroxenes. Given the extremely dry nature of lunar basalts, fluid activity cannot explain the Li-B rim depletions observed in this study. However, Li and B distributions are influenced by changes in mineral composition during crystallization, shock pressure and subsequent thermal metamorphism.

References: [1] Johnson, M.C. et al. (1991) *GCA*, 55, 349-366. [2] Mysen, B.O. et al. (1998) *Am. Min.*, 83, 942-946. [3] McSween, H.Y. Jr. & Harvey, R. P. (1993) *Science* 259, 1890-1892. [4] Dann, J.C. et al. (2001) *MAPS*, 36, 793-806. [5] McSween, H.Y. et al. (2001) *Nature*, 409, 487-490. [6] Lentz, R.C.F. et al. (2001) *GCA*, 65, 4551-4565. [7] Chaklader, J. et al. (2004) *LPSC XXXV*, abstr. 1397. [8] Fritz, J. et al. (2003) *LPSC XXXIV*, abstr. 1335. [9] Schaal, R.B. and Horz, F. (1977) *Lunar Sci. Conf. 8th*, 1697-1729. [10] Nyquist, L.E. et al. (1991) *LPSC XXII*, 985-986. [11] Nyquist, L.E. et al. (1991) *LPSC XXII*, 987-988. [12] BVSP (1981) *Pergamon Press*, 371-384. [13] Bence, A. E. & Papike, J. J. (1972) *Lunar Sci. Conf. 3rd*, 431-469. [14] Herd et al. (2004) *Am. Min.*, 832-840.

Acknowledgements: L. Borg, Z. Sharp, R. Jones & M. Ali helped with heating experiments. M. Spilde helped with SEM & EMP analyses. The NASA Mars Fundamental Research Program provided funding for this study.

Figure 1. Variation in quadrilateral components for A-11 pyroxenes.

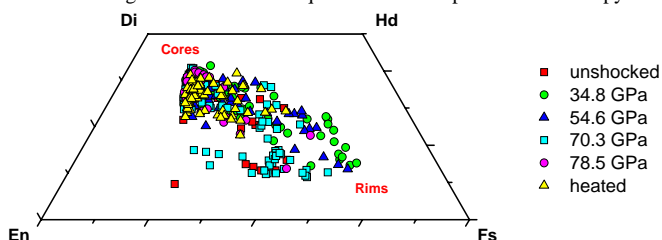


Figure 2. Variation in quadrilateral components for A-17 pyroxenes.

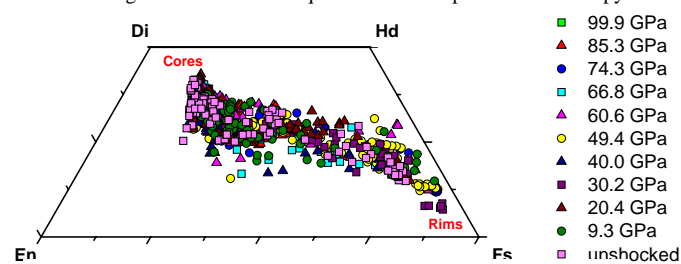


Figure 3. Ti vs. Al plot for A-17 pyroxenes.

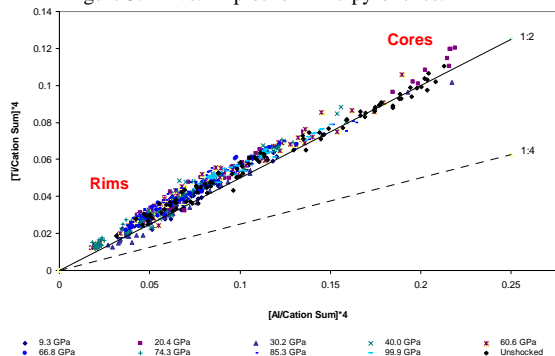


Figure 4. Al/Si vs. Wo-content plot for A-17 pyroxenes.

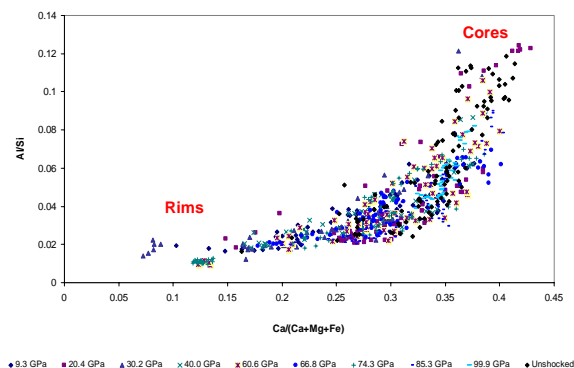


Figure 5. Li (ppm) vs. Li/Ce plot for A-17 pyroxenes.

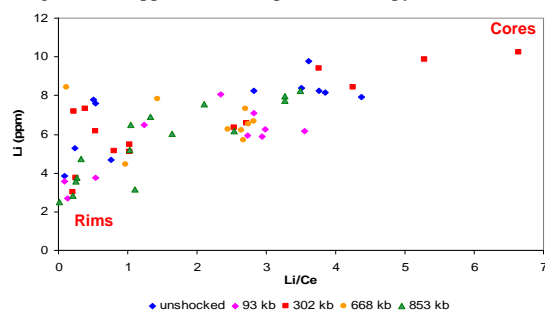


Figure 6. B (ppm) vs. B/Ce plot for A-11 & A-17 pyroxenes.

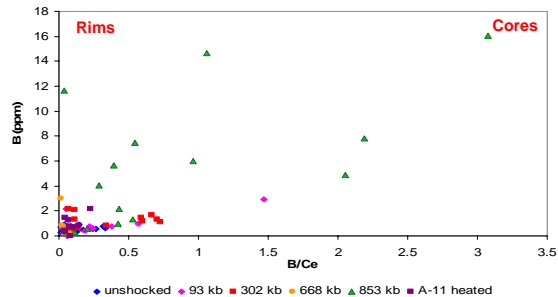


Figure 7. Li (ppm) vs. Wo-content for A-17 pyroxenes.

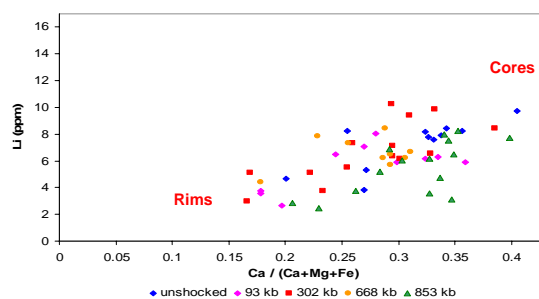


Figure 8. (Al³⁺)^{VI} vs. Li (ppm) plot for A-11 & A-17 pyroxenes.

